Surface & Coatings Technology 404 (2020) 126480

Contents lists available at ScienceDirect

Surface & Coatings Technology

journal homepage: www.elsevier.com/locate/surfcoat

Laser surface polishing of NiCrSiBC – 60WC ceramic-metal matrix composite deposited by laser directed energy deposition process

Amit Choudhary[a], Abhijit Sadhu[b], Sagar Sarkar[b], Ashish Kumar Nath[b], Gopinath Muvvala[a,*]

[a] Department of Mechanical and Aerospace engineering, Indian Institute of Technology Hyderabad, 502285, India
[b] Department of Mechanical Engineering, Indian Institute of Technology Kharagpur, 721302, India

ARTICLE INFO

Keywords:
Laser surface polishing
Directed energy deposition
Ceramic-metal composite
Molten pool thermal history
Surface roughness

ABSTRACT

Deposition of ceramic-metal matrix composite using laser directed energy deposition process presents multi-fold challenges. High melting point ceramic particles often remain partially melted and increase the roughness of the deposit, which essentially requires secondary finishing operation. Besides high surface roughness, the high gradient of thermal and physical properties between ceramic reinforcement and metal matrix introduces cracks in the composite. Therefore, in the present work, the effect of laser surface polishing and substrate heating on improving the surface quality of NiCrSiBC – 60WC ceramic-metal composite deposited by laser directed energy deposition process was investigated. The molten pool thermal history was monitored using an IR pyrometer during laser surface polishing. The effect of rate of heat input on heating rate, cooling rate, molten pool lifetime and peak temperature was investigated and correlated with the surface quality parameters viz. arithmetic surface roughness (Ra) and ten-point height (Rz). A combination of intermediate laser power and scanning speed (600 W and 2000 mm/min) resulted in proper spread of molten pool and rendered better surface finish. The surface roughness (Ra) was found to improve from 19.2 μm ± 1.36 to 1.75 μm ± 0.20. Further, different orientations of laser polishing (0°, 45°and 90°) with respect to the material deposition direction were examined, and 45° was found to yield better surface finish. Surface cracks were observed for all the cases irrespective of process parameters and cooling rates, which were mitigated by substrate pre-heating.

1. Introduction

Laser directed energy deposition (L-DED), in the frame of additive manufacturing (AM), is receiving an increasing interest for refurbishment of worn out components and development of protective coatings including ceramic-metal composite coatings over other traditional techniques [1–3]. This is due to the fact that the L-DED process involves high power densities with localized rapid heating and melting of material with minimum heat flowing into the substrate followed by rapid cooling by self-quenching due to large thermal gradients. However, the components deposited using L-DED process cannot be used directly owing to their poor surface finish and essentially require secondary finishing operations [4].

In recent years, laser surface polishing has become popular for surface finishing operation of components manufactured by additive technique [5,6]. The laser surface polishing process is very similar to laser remelting, wherein remelting is carried out in a controlled way so that the liquid metal is redistributed between peaks and valleys due to surface tension and gravity followed by rapid solidification reducing the surface roughness. Chen et al. [7] investigated the effect of laser power, scanning speed and spot diameter on formation of bulge structure in laser surface polishing of Ti-6Al-4V and attributed it to the volume expansion related to phase transformation and mass transformation. They [7] also observed better surface finish for higher overlapping percentage. Dai et al. [8] investigated the effect of laser fluence during laser polishing of SKD 11 tool steel on rough surfaces produced by electric discharge machining and milling process. Laser fluence beyond a critical limit found to have a detrimental effect due to surface over melting while below this value, the surface was found to be in shallow surface melting regime reducing the surface roughness [9]. Similarly, Temmler et al. [10] investigated the effect of shielding gas during laser surface polishing of H11 tool steel and reported higher arithmetic roughness (Ra) value while using Ar as shield gas compared to Ar + O_2 + CO_2. This was attributed to the formation of martensitic phase transformation causing bulging in case of Ar as shielding gas. Yung et al. [11] investigated the effect of laser surface polishing on complex surface geometries prepared by additive manufacturing and proposed a method of layered polishing for complex geometries in

* Corresponding author at: Department of Mechanical and Aerospace Engineering, IIT Hyderabad, 721302, India.
E-mail address: mgopinath@mae.iith.ac.in (G. Muvvala).

https://doi.org/10.1016/j.surfcoat.2020.126480
Received 25 July 2020; Received in revised form 30 September 2020; Accepted 5 October 2020
Available online 10 October 2020

Table 1
L-DED process parameters.

Laser power P (W)	Scanning speed V (mm/min)	Powder mass flow rate ṁ (g/min)	Spot diameter (mm)	% overlap	Carrier, shrouding and shielding gas flow rate (L/min)
600	700	25	1.6	50	20, 20, 5

Table 2
Laser polishing process parameters.

Process parameters set	Laser power P (W)	Scanning speed V (mm/min)	Line energy P/V (J/mm)	Spot diameter (mm)	Remelt angle θ (°)	% overlap	Shielding gas flow rate (L/min)
Set 1	300	1000	18	2	0, 45, 90	50	20
Set 2	600	2000					
Set 3	900	3000					

addition to parametric optimization. In another work, Yung et al. [12] demonstrated the possibility of generating hydrophilic and hydrophobic surface on additively manufactured CoCr. Wang et al. [13] further improved the corrosion properties of CoCr by laser surface polishing. Marimuthu et al. [14] carried out laser surface polishing of Ti-6Al-4V samples prepared by selective laser melting (SLM) and demonstrated the possibility of improving the surface roughness without affecting the mechanical properties or structure of the material. Similar to Dai et al. [8], Marimuthu et al. [14] also observed an increase in the surface roughness with laser energy and this was attributed to surface over melting due to increased melt pool velocity and increased periodic striation patterns which they evaluated based on computational fluid dynamic formulation. Tian et al. [15] studied the effect of laser polishing on grain structure, texture and surface roughness of additively manufactured Ti-6Al-4V by electron beam. Surface properties of Ti-6Al-4V were found to be retained within the remelted zone owing to decomposition of martensitic phase to a very fine α + β lamellae structure due to subsequent beam passes [15]. Li et al. [16] reported the possibility of reduction in surface porosity of Inconel 718 by 65.7% compared to as-deposited samples by selective laser melting. Dadbakhsh et al. [17] evaluated the effect of laser power, scanning speed and spot diameter during laser polishing to improve the surface roughness of Inconel 718 deposited by L-DED process. Rosa et al. [18] also investigated the surface quality of laser polished thin and intricate parts manufactured by L-DED process and reported the improvement in surface quality with number of passes. Further, the multi-pass scanning strategy was reported to mitigate the cracks observed in the first pass [18].

It may be observed that most of the studies reported above are either related to polishing of conventionally machined samples or samples additively manufactured by selective laser remelting. However, the studies related to laser polishing of component fabricated by L-DED process are limited. Further, most of the studies are related to metal systems. Thus the present study investigates the effect of laser surface polishing on ceramic-metal composite coatings of NiCrSiBC – 60WC deposited by L-DED process. Additionally, it may be observed that in most of the afore-mentioned literature, process parameters like laser power, scanning speed and spot diameter were varied. However, the efficient redistribution of material between peaks and valleys depend on the molten pool lifetime and cooling rate. Therefore, in the present study the molten pool thermal history is monitored using an IR pyrometer and correlated with resulting surface roughness which also gives an assessment of surface over melting and shallow surface melting. Further, it is possible to have different cooling rates for the same amount of heat input but at different rate [19,20]. Hence, laser polishing in the present work is carried out using same line energy at different heat input rates. Also, the effect of polishing direction with respect to the initially deposited tracks is investigated. Unlike metal systems, ceramic-metal composite coatings suffer from surface cracks due to high residual stresses experienced from large variation in the thermo-physical properties of the metal matrix and ceramic particles when rapidly melted and solidified [20,21]. Thus the effect of substrate preheating on mitigation of cracks is also investigated.

2. Experimental setup

A 2 kW Yb-fiber laser integrated with an in-house fabricated co-axial laser cladding head, mounted on a 5-axis CNC was used for both directed energy deposition and laser polishing. A 16 mm diameter collimated beam was focused down to the desired spot dimeter using a 200 mm focal length plano-convex lens. A twin hopper powder feeder (Model: MPF – 700T, Make: M/S MC Thermal Spray Equipment, India) was used for feeding the powder material into the co-axial laser cladding head. The stand-off distance (SOD) was maintained at 10 mm with 1.6 mm as the laser spot diameter on the substrate surface during L-DED process. In case of laser remelting, however, the SOD was increased to 40 mm and a spot diameter of 2 mm was maintained on the deposited coating. Process parameters used for L-DED and laser surface polishing are shown in Tables 1 and 2. The scanning strategies used for laser surface polishing, i.e. 0°, 45° and 90°, where 0° angle corresponds to polishing in the same direction of deposition, are shown in Fig. 1.

Inconel 718, a nickel based super alloy widely used in the hot sections of rocket engines such as pre-burner exhaust, combustion chamber inlet and turbine blades etc. [4], was used as the substrate. NiCrSiBC – 60%WC, a pre-alloyed hardfacing powder with spherical morphology and size range of 45–90 μm (Fig. 2) was used as the coating material. Table 3 and Table 4 show the chemical composition of the substrate and the powder material, respectively. Argon gas was used as carrier, shrouding and shielding gas. Prior to deposition, Inconel 718 substrates (50 mm × 25 mm × 8 mm) were grit blasted and cleaned in ultrasonic bath of ethanol. For substrate heating, a resistance heater controlled by variable auto-transformer was used [21]. An IR pyrometer (Micro Epsilon, model: CTLM-2HCF3-C3H) operating at 1.6 μm wavelength fitted with a 1064 ± 25 nm notch filter to block the reflected laser radiation was used to record the molten pool thermal history [21]. The pyrometer operates at 1 kHz frequency and acquires temperature signal from 0.7 mm diameter zone with measuring temperature range as ~785–3260 °C.

Surface morphology was investigated using Zeiss – EVO 18 Research scanning electron microscope (SEM) and the surface roughness was measured using a contact type 3D profilometer (Make: Taylor Hobson, Model: Form Talysurf 50 Intra 2). An area of 10 mm × 10 mm was scanned for measuring the surface roughness. In order to investigate the cross-sectional morphology and melt depth, the sample were cut using a wire-cut EDM and mirror polished with P400 to P2000 grade SiC paper, followed by 1 μm diamond paste and analyzed under the SEM. Further hardness test was carried out using Vickers hardness tester (Walter UHL, model: VMH-001) with 100 g load and 15 s dwell time.

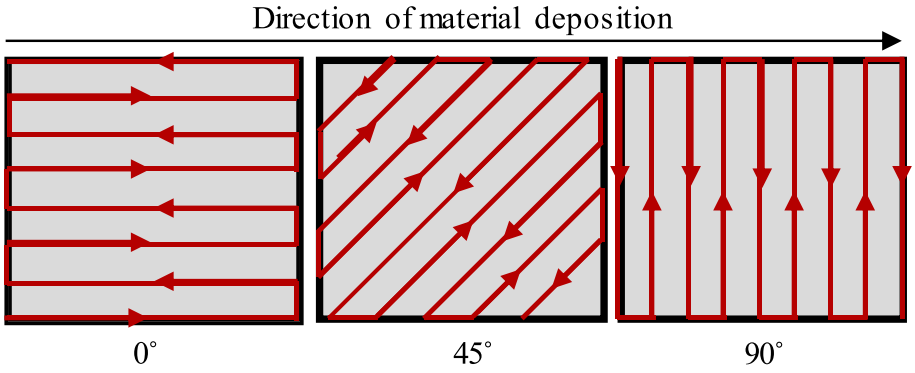

Fig. 1. Laser polishing scanning strategy.

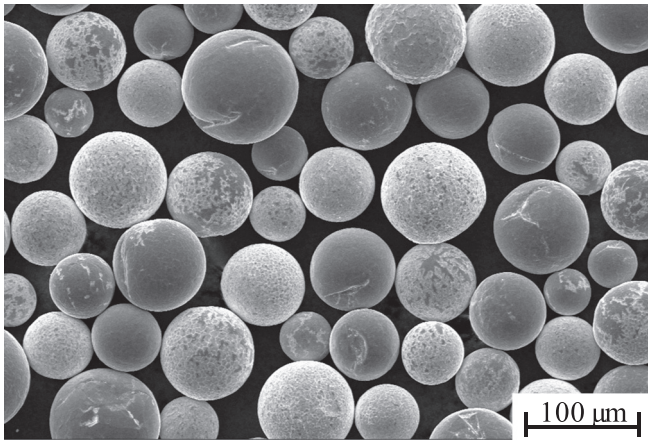

Fig. 2. Morphology of powder material.

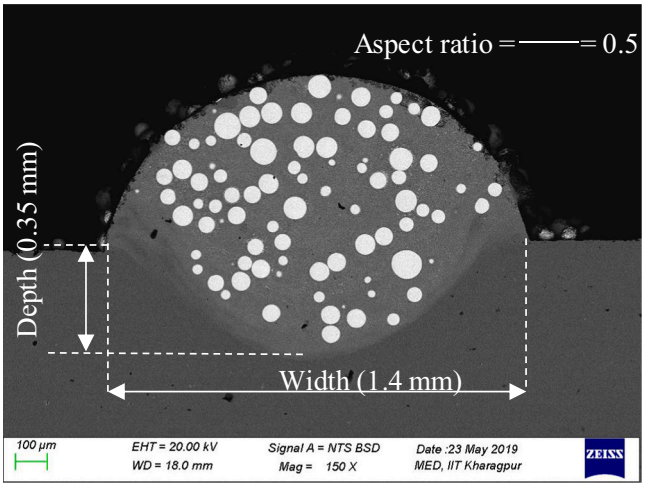

Fig. 3. Single bead cross-section corresponding to parameters in Table 1.

Table 3
Chemical composition (wt%) of substrate material.

Element (wt %)	Cr	Fe	Nb	Mo	Al	Ti	Mn	Si	B	Ni
IN 718	19.02	18.1	4.92	3.19	0.54	0.97	0.04	0.20	0.004	Bal.

3. Results and discussion

3.1. Surface morphology of as deposited samples

As discussed in Section 1, the mechanism of formation of surface roughness or waviness is very different in case of directed energy deposition and selective laser melting. In case of SLM, typical power densities defined as laser power divided by irradiation area ($^{4P}/_{\pi D^2}$) where 'D' is the laser spot diameter, are in the range of 1.5×10^5–3.5×10^5 W/mm^2 [11], while it is in the range of 0.7×10^3–2.5×10^3 W/mm^2 [17] in case of L-DED. Moreover, in most of the SLM systems, fiber lasers with Gaussian beam intensity profile are used. Hence, key hole formation is predominant in case of SLM due to high power densities and Gaussian beam intensity profile where vapour pressure cause axisymmetric periodical harmonic perturbation driving the molten pool into instability leading to surface undulations with defined parametric dependent wavelength [22,23]. However, in case of L-DED process, the chances of key hole formation are very less and this is also evident from the bead geometry shown in Fig. 3 where the aspect ratio of bead depth to half of width is less than 1 (0.5) representing the dominance of conduction mode [22,24].

In case of L-DED process, unlike SLM, the powder continuously gets deposited into the molten pool created by a fraction of laser beam that passes through the powder cloud [25,26]. As the laser beam advances, the molten pool starts solidifying and the powder that comes in contact at the verge of solidification, sticks to the surface with partial melting as shown schematically in Fig. 4. The actual surface morphology of as deposited sample is shown in Fig. 5(a) and (b), from which it is evident that poor surface finish in case of L-DED process is essentially due to partially melt particles on the surface. The partial melting is more dominant in case of ceramic-metal composites where the melting point of ceramic material is high. Moreover, the deposition rates in L-DED are high compared to SLM causing regular interval oscillations due to overlapping tracks as shown in Fig. 4. These regular interval oscillations, called waviness, are excluded from calculating the roughness value in most of the surface roughness measuring techniques or

Table 4
Chemical composition (wt%) of powder material.

Element (wt%)	Hard phase wt% (60%)			Metal matrix wt% (40%)					
	W	C	Fe	Ni	Cr	Si	B	Fe	C
NiCrSiBC	Bal.	3.8	< 0.3	Bal.	6.8–8.3	3.1–3.9	1.4–1.9	1.7–3.3	0.1–0.4

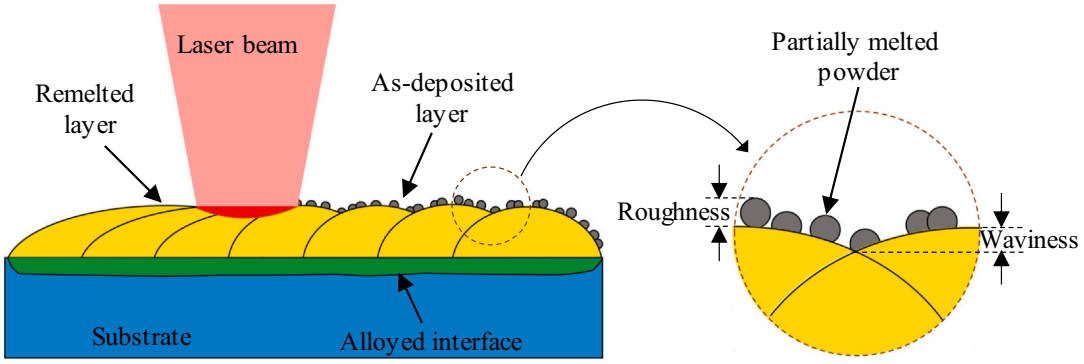

Fig. 4. Schematic view of laser polishing.

instruments. However, waviness is also detrimental parameter in affecting the component life or its use in real-time applications. In subsequent sections, the effect of laser polishing on these parameters is discussed in detail.

3.2. Effect of process parameters on molten pool thermal history

The efficacy of laser polishing in reducing the surface roughness depends on the volume of the molten pool, its wetting characteristics and the solidification time available. Higher energy would melt more surface creating larger melt pool ensuring melt flow and proper wetting on the surface. However, the solidification rate also greatly affects spreading or wetting of the molten pool and plays a crucial role in controlling the humping [22,24]. As conduction is the main mode of heat transfer in establishing the molten pool and controlling the solidification process in L-DED, the rate at which the energy is supplied (heating rate) greatly affects the surface roughness. Therefore, to investigate the effect of rate of heat input on solidification or molten pool lifetime and resulting surface roughness, laser power and scanning speed were varied keeping the line energy constant at 18 J/mm according to the laser parameters given in Table 2.

Fig. 6(a) shows a typical molten pool thermal cycle recorded during laser polishing at 900 W laser power and 3000 mm/min scanning speed. The molten pool thermal history consisted of two cycles namely heating cycle (0A) and cooling cycle (AD). In laser polishing, as the laser beam irradiates on the sample, the surface temperature rises rapidly above the melting point of the material and reaches to a peak value depending upon the parameters. This phase represents the heating cycle (0A). The heating rate is determined from this cycle by using Eq. (1), where T_o, T_1, t_o and t_1 are initial pyrometer detectable temperature, surface peak temperature, start time and time took to reach peak temperature, respectively. As the laser proceeds, the molten pool behind the laser beam starts cooling, solidifies and reaches to room temperature, represented by cooling cycle (AD). The time taken by molten pool to reach the solidus temperature (T_2) of the material from surface peak temperature represents the molten pool lifetime (AC) calculated using Eq. (2). In the present study, the solidus temperature of NiCrSiBC (T_2) was used to calculate the molten pool lifetime as shown in Fig. 6(a). Further, the cooling rate is determined by the temperature gradient between solidus temperature and the pyrometer detectable temperature as shown in Eq. (3).

$$Heating\ rate = \frac{T_1 - T_0}{t_1 - t_0}\ (°C/s) \quad (1)$$

$$Molten\ pool\ liftime = t_2 - t_1\ (ms) \quad (2)$$

$$Cooling\ rate = \frac{T_2 - T_0}{t_3 - t_2}\ (°C/s) \quad (3)$$

Fig. 6(b) shows the variation in molten pool thermal cycle at 0° scanning orientation corresponding to the process parameters listed in Table 2. Though the line energy was kept constant at 18 J/mm for all the three cases, it can be observed that there is a significant difference in the molten pool thermal cycle profile. Fig. 7 and Table 5 summarizes the variation in different aspects of molten pool thermal history i.e. heating rate, cooling rate, molten pool lifetime and surface peak temperature with respect to the process parameters. The heating rate showed an increasing trend with the combination of increasing laser power and scanning speed (Fig. 7(a)).The heat input rate is generally controlled by laser scanning speed which defines the interaction time τ ($\frac{Laser\ spot\ diameter}{Scanning\ speed}$) of the laser with substrate at a given point. For a given line energy, at higher scanning speeds the whole energy is transferred to the substrate within a shorter duration, rising the temperature rapidly compared to the lower scanning speeds. It can also be observed that cooling rate too followed a similar trend as heating rate (Table 5). As discussed, due to rapid heat input the energy is absorbed in a thin layer with minimum heat conduction, establishing higher gradients

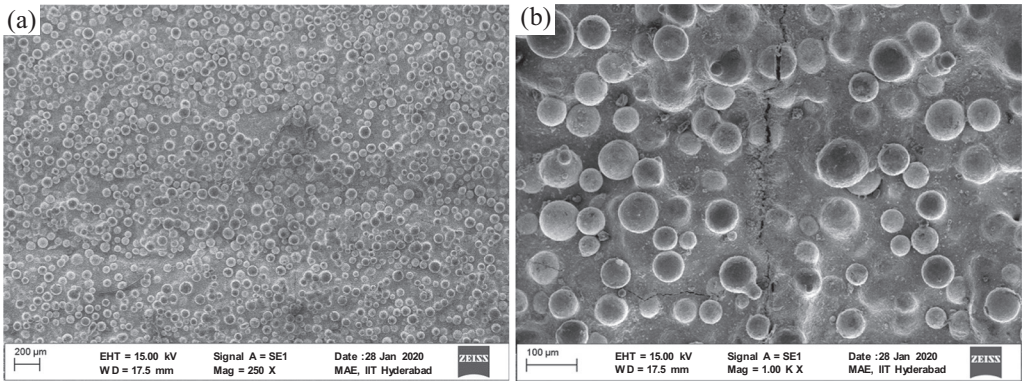

Fig. 5. Surface morphology of as deposited sample corresponding to parameters in Table 1.

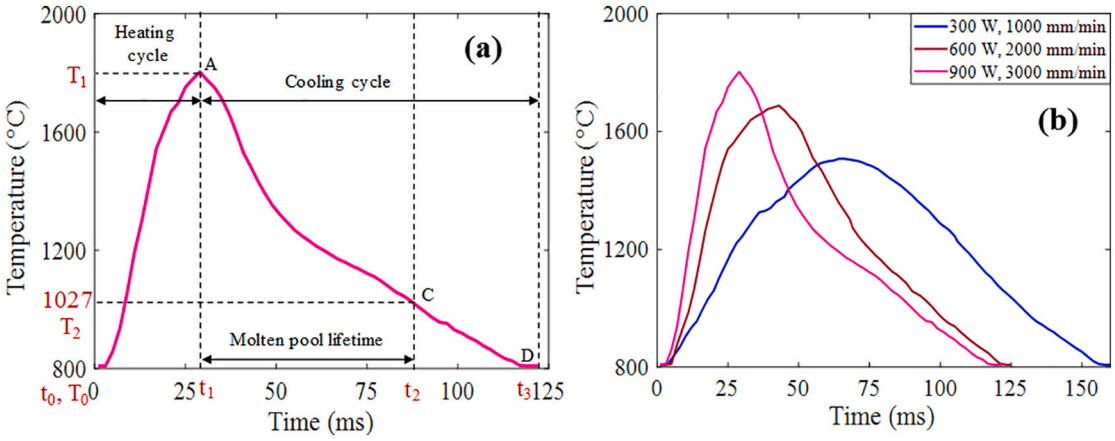

Fig. 6. (a) Different features in molten pool thermal cycle and (b) variation in thermal cycle profile with process parameters.

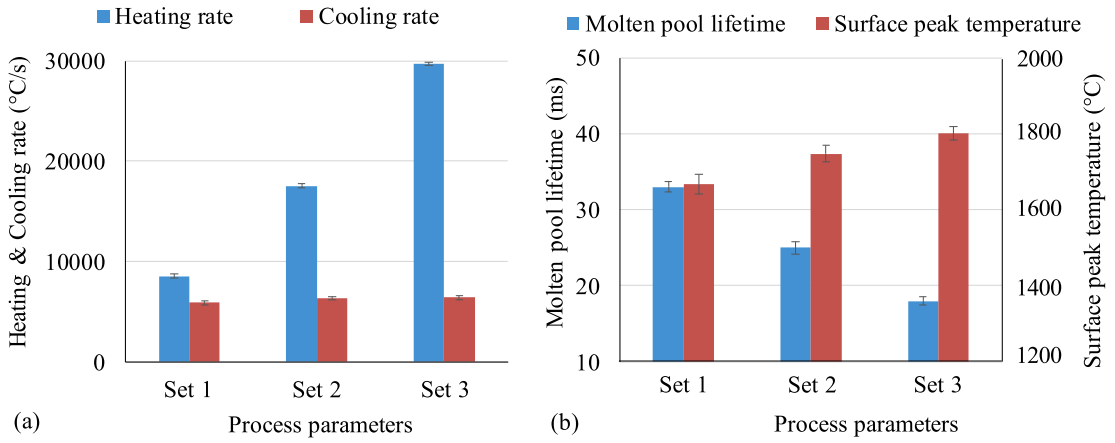

Fig. 7. Effect of process parameters on (a) heating and cooling rate and (b) molten pool lifetime and surface peak temperature.

Table 5
Variation in heating and cooling rate, and molten pool lifetime with process parameters (mean values).

Set	Process parameters	Heating rate (°C/s)	Cooling rate (°C/s)	Molten pool lifetime (ms)	Surface peak temperature (°C)	Melt depth (~μm)
Set 1	300 W, 1000 mm/min	8.5×10^3	5.9×10^3	33	1500	81
Set 2	600 W, 2000 mm/min	17.5×10^3	6.3×10^3	25	1680	154
Set 3	900 W, 3000 mm/min	29.7×10^3	6.4×10^3	18	1800	194

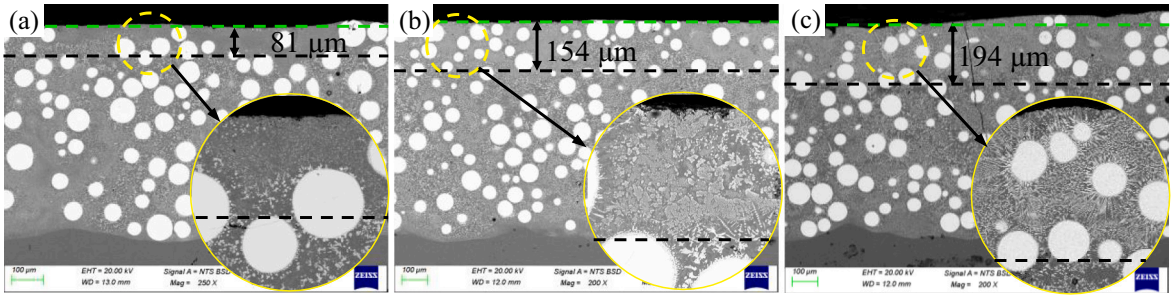

Fig. 8. Variation in melt depth with process parameters at 0° orientation (a) 300 W, 1000 min, (b) 600 W, 2000 mm/min, (c) 900 W, 3000 mm/min.

with the substrate leading to faster cooling rates. It can also be observed that the surface temperature is high in case of set 3 process parameters. The molten pool lifetime was found to be higher in case of set 1 (Fig. 7(b)) where the cooling rate was the least (Fig. 7(a)). It is interesting to note here that the melt depth in case of set 1 is lower than other 2 cases as shown in Fig. 8. In general, molten pool lifetime increases with increase in its size. In the present work, however, it can be observed that at lower molten pool size or depth, the molten pool lifetime was found to be higher. The expression to estimate the molten pool lifetime with respect to its size is given in Eq. (4) [22], where τ_m, s, a, K, K_{sub}, T_i, T_{sub}, T_L, L, C correspond to molten pool lifetime (s), initial droplet size (m), thermal diffusivity (m^2/s), thermal conductivity of the molten pool (W/m K), thermal conductivity of the substrate (W/m K), initial temperature of droplet (peak temperature in current case),

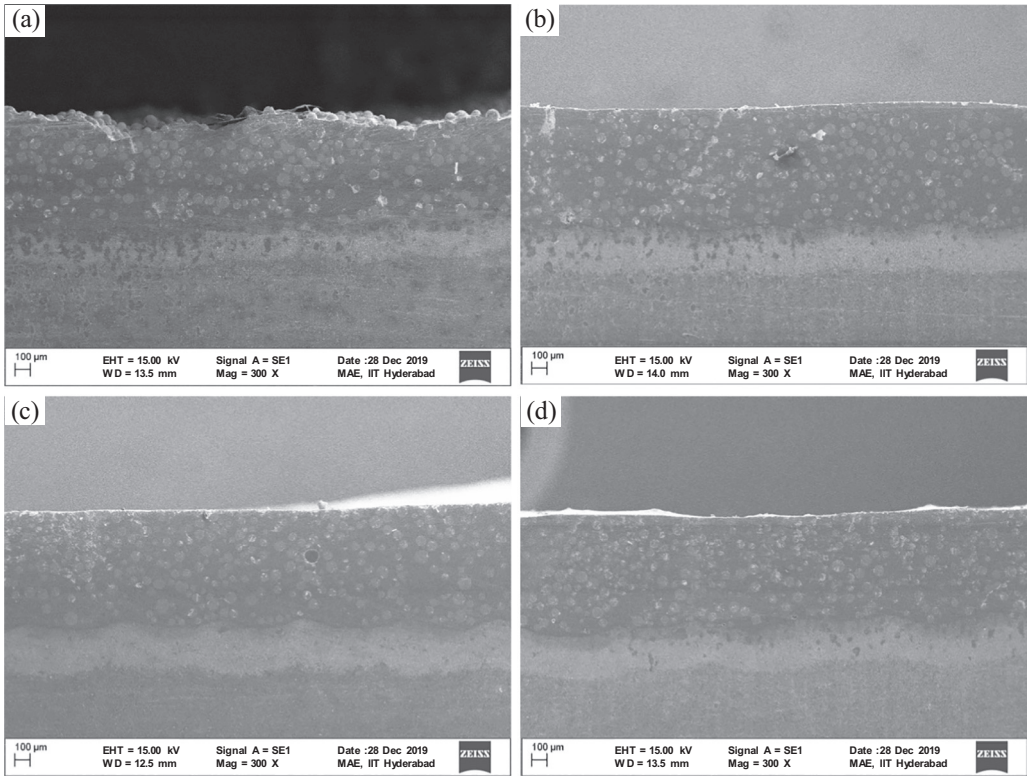

Fig. 9. Cross-sectional view of (a) as-deposited, and laser polished surface at 0° orientation at (b) 900 W, 3000 mm/min, (c) 600 W, 2000 mm/min and (d) 300 W, 1000 mm/min.

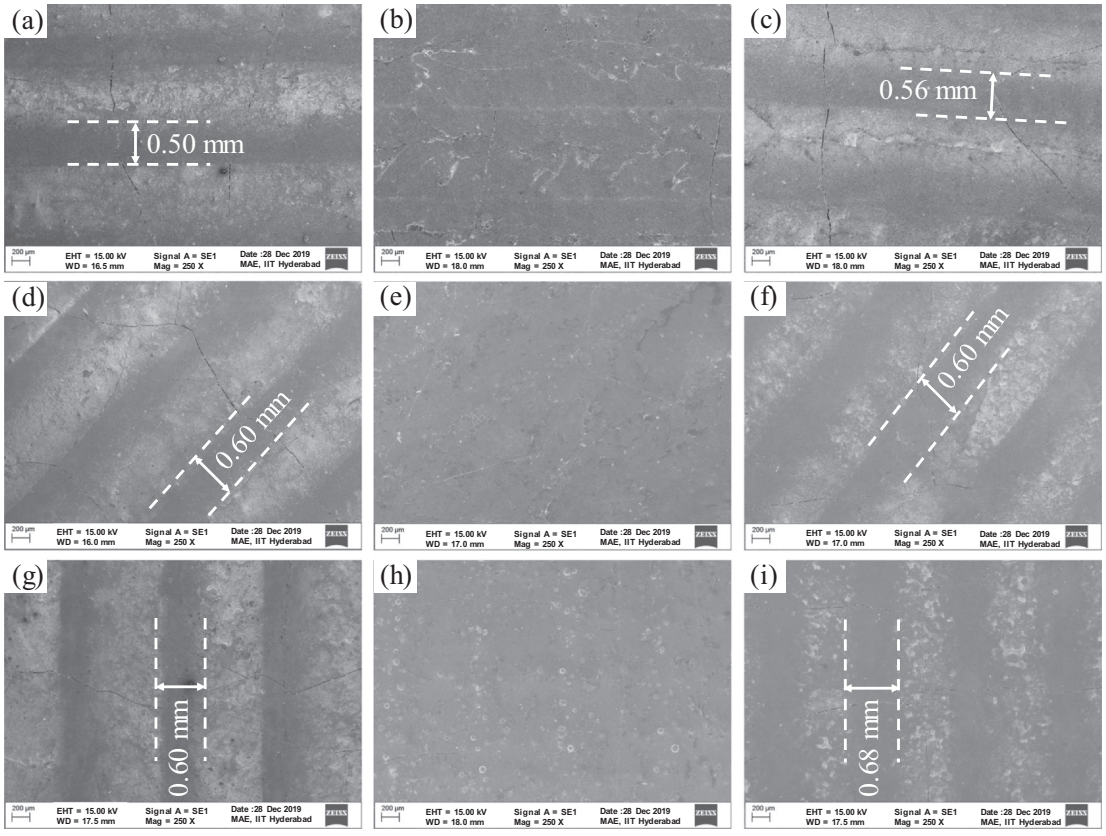

Fig. 10. Surface morphology of laser polished samples at an angle of (a)–(c) 0°; (d)–(f) 45°; (g)–(i) 90° at laser power and scanning speed of (a), (d), (g) 900 W, 3000 mm/min; (b), (e), (h) 600 W, 2000 mm/min; and (c), (f), (i) 300 W, 1000 mm/min.

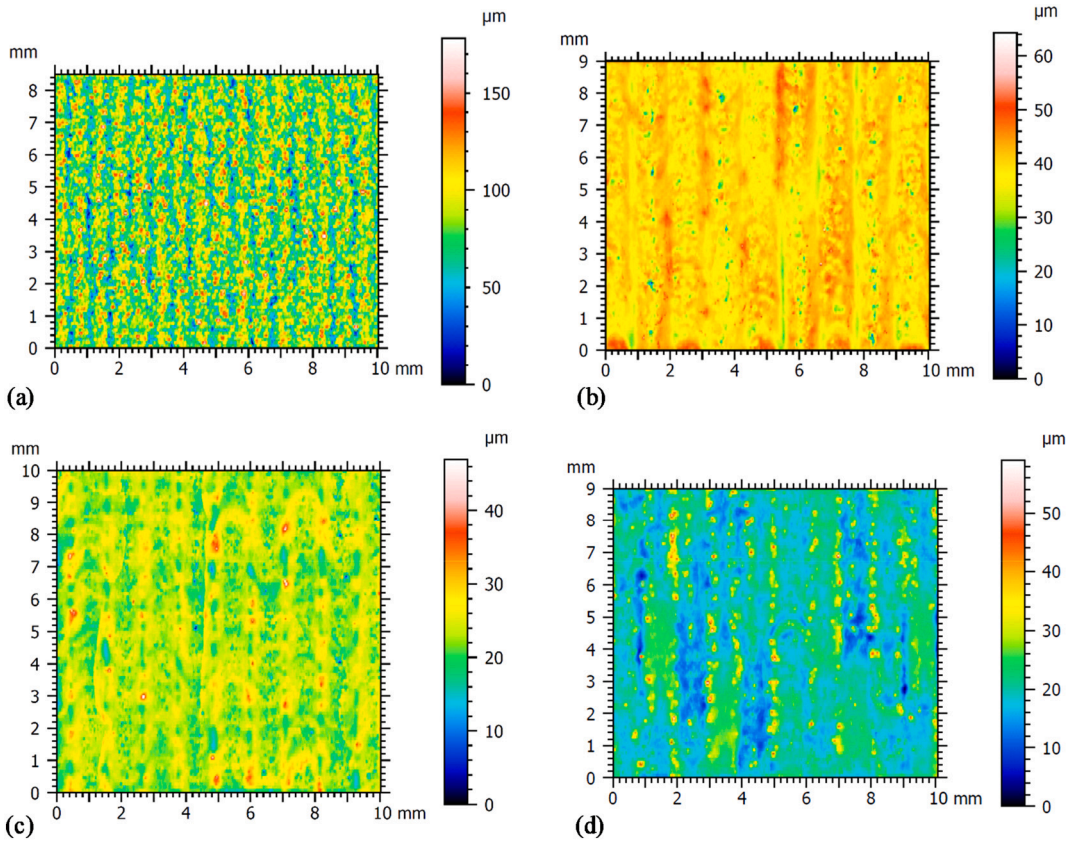

Fig. 11. Surface topography images of (a) as deposited and samples polished at 0° and (b) 900 W, 3000 mm/min, (c) 600 W, 2000 mm/min and (d) 300 W, 1000 mm/min.

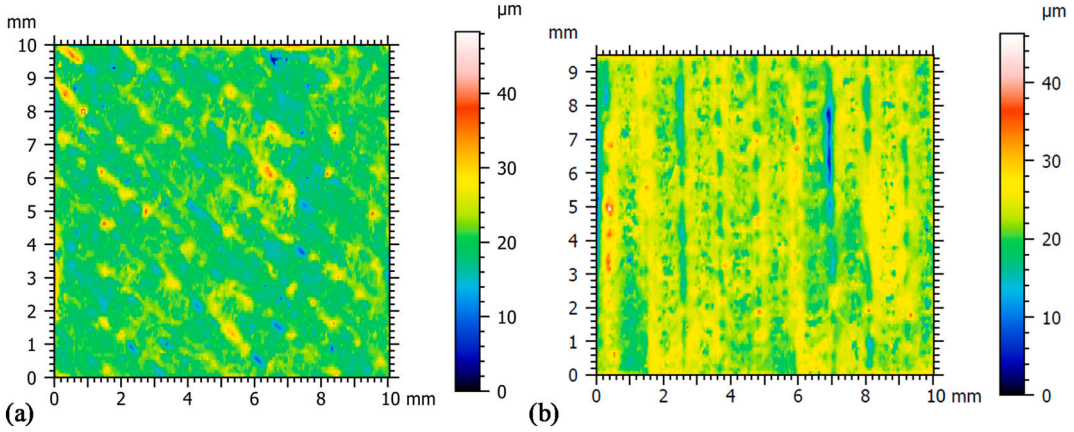

Fig. 12. Surface topography images of samples remelted at 600 W laser power, 2000 mm/min scanning speed at (a) 45° and (b) 90°.

substrate temperature, liquidus temperature, substrate length, and specific heat capacity, respectively. From this expression, it can be inferred that the molten pool lifetime also depends on substrate temperature which for the present work is dependent on the scanning speed. With decrease in scanning speed to 1000 mm/min from 3000 mm/min, the interaction time of laser with deposited surface increases to 180 ms from 60 ms. At higher interaction time with reduced laser power, the loss of energy due to conduction is dominant resulting in reduction of peak surface temperature as observed in Fig. 6(b). Further, the temperature of substrate rises and this decreases the temperature gradient resulting in longer molten pool lifetime as shown in Fig. 6(b). The effect of these aspects on surface roughness is discussed in the next section.

$$\tau_m = \frac{s^2 K}{3aK_{sub}}\left[\ln\left(\frac{T_i - T_{sub}}{T_L - T_{sub}}\right) + \left(1 + \frac{K_{sub}}{2K}\right)\frac{L}{C(T_L - T_{sub})}\right] \quad (4)$$

3.3. Effect of process parameters on surface roughness

Fig. 9 shows the cross-section of as deposited and laser surface polished samples at different process parameters. As discussed previously, in case of as deposited sample (Fig. 9(a)), it can be observed that on the surface there are particles sitting which are partially melt and the surface is exhibiting the waviness due to the overlapping tracks. After laser surface polishing (Fig. 9(b)–(d)), it can be observed that a controlled melting of surface took place without formation of any humps or bulges as the power densities that are used for laser polishing are in the

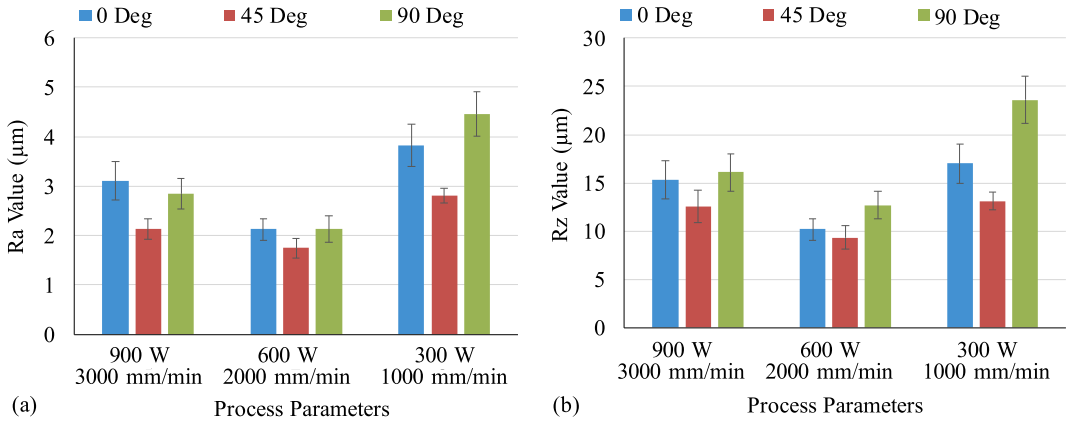

Fig. 13. Variation in (a) R_a and (b) R_z with process parameters.

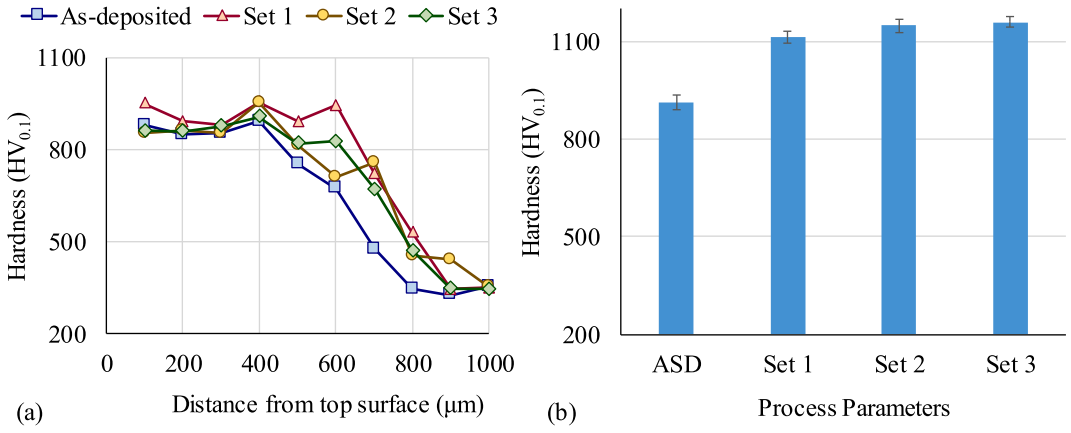

Fig. 14. Variation in hardness (a) along the depth and (b) on the laser polished samples with 0° scan orientation.

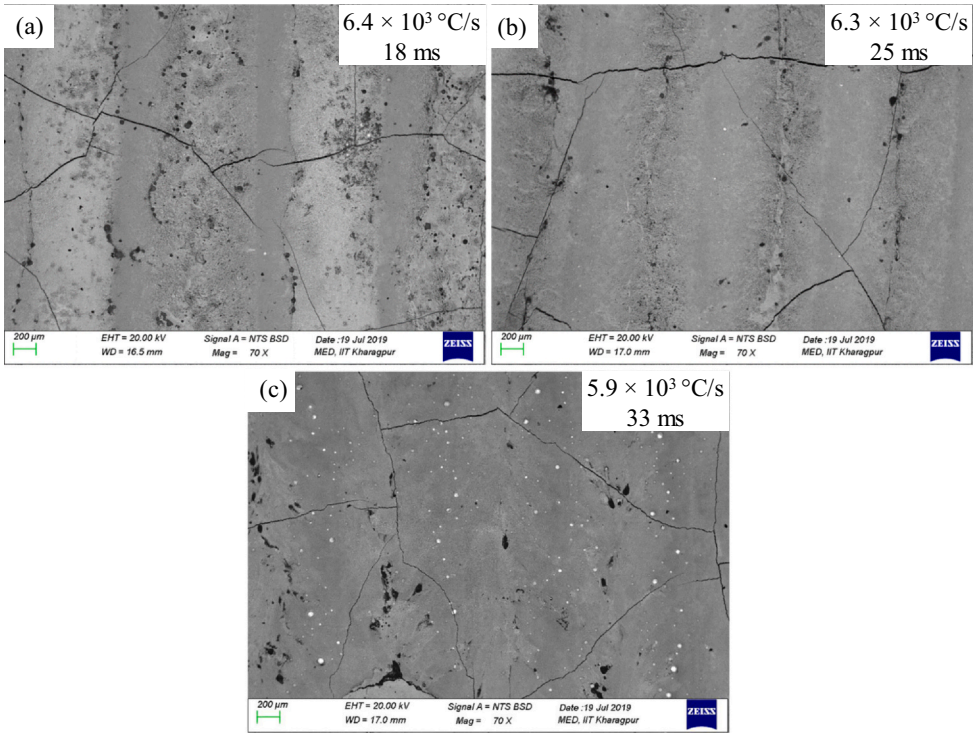

Fig. 15. BSE images showing the surface cracks (a) 900 W, 3000 mm/min, (b) 600 W, 2000 mm/min and (c) 300 W, 1000 mm/min (0° orientation).

Table 6
Material properties [27,28].

Material	Thermal expansion coefficient (10^{-6} K^{-1})	Elastic modulus (GPa)	Melting temperature (K)
NiCrSiBC	13.3–16.8	200–240	1300
WC	6.5–7.4	650–710	3140

range of ~96–287 W/mm^2 which is much less compared to that discussed in Section 3.1. However, it may be observed that in case of 900 W laser power and 3000 mm/min scanning speed (Fig. 9(b)), the surface still exhibited slight waviness. This could be attributed to lower molten pool lifetime resulting in relatively poor spreading compared to other two cases. Fig. 10 shows the surface morphology of the samples polished at 0°, 45° and 90° for all the combinations of laser powers and scanning speeds. It may be interesting to observe that irrespective of orientation, polishing marks with a gap close to half of the track width were evident in case of 900 W, 3000 mm/min and 300 W, 1000 mm/min combinations as shown in Fig. 10(a), (d), (g) and (c), (f), (i) respectively. This may be attributed to lower molten pool lifetime and higher loss of energy due to conduction in case of 900 W, 3000 mm/min and 300 W, 1000 min respectively, leading to relatively poor spreading. However, in case of 600 W, 2000 mm/min combination, the surface appeared smooth and uniform. Fig. 11 shows the surface topography of the as deposited (Fig. 11(a)) and laser polished samples (Fig. 11(b)–(d)) at 0° orientations. As discussed in Fig. 5, it can be observed from Fig. 11(a) that the surface of as deposited sample is quite rough with Ra and Rz values as 19.2 μm ± 1.36 and 91.9 μm ± 5.67 respectively. It is interesting to note that Rz value in as deposited sample is close to that of maximum particle size used in the present work. Further, it may be observed that the surface quality is poor in case of 900 W and 3000 mm/min combination (Fig. 11(b)) compared to the other two. Though 300 W and 1000 mm/min combination seems to provide better surface finish, it is observed that the surface exhibited undulation in wide range (blue to red colour). Set 2 was found to provide an optimum Ra values. Fig. 12 shows the variation of surface topography for set 2 under different orientation of laser polishing and Fig. 13 summarizes the variation in Ra and Rz values with respect to both laser power and scanning speed combination and orientation of laser polishing. It can be inferred from Fig. 13 that irrespective of polishing orientation, 600 W laser power and 2000 mm/min scanning speed resulted in a better surface finish because of the optimum molten pool lifetime and cooling rate as discussed earlier. Further, it may be observed that among all the combinations of laser powers and scanning speeds, 45° polishing orientation was found to yield better surface finish followed by 0° orientation. In the present study, the laser spot diameter for polishing was set at 2 mm such that at a given instant it covered two peaks and one valley allowing a proper redistribution of material between the valley and peaks. However, this holds true only in case of 0° orientation. In case of 90° orientation, as the CNC moves, laser beams continuously changes from peak to valley or vice versa creating an unstable molten pool resulting in poor surface finish. Thus, compared to 90° orientation, laser polishing in 0° orientation resulted in better surface quality. The results in case of laser polishing at 45° orientation showed further improvement in the surface roughness as shown in Figs. 12 and 13. At 45° orientation, similar to 0° orientation, laser beam simultaneously melts peaks as well as valleys. However, at 45° orientation, the clad track width is $\sqrt{2}$ times the actual width which decreases the slope of the waviness and allows formation of stable molten pool with easy spreading. Therefore, 600 W laser power and 2000 mm/min scanning speed combination with optimum molten pool lifetime and 45° orientation could effectively reduce the Ra and Rz of as deposited samples from 19.2 μm ± 1.36 and 91.9 μm ± 5.67 to 1.75 μm ± 0.20 and 9.3 μm ± 1.22, respectively.

In addition to the surface roughness, hardness test was carried out to investigate the effect of laser polishing on the hardness of ceramic-metal matrix composite coatings. Fig. 14 shows the effect of laser surface polishing on hardness in case of set 1–3 process parameters with 0°

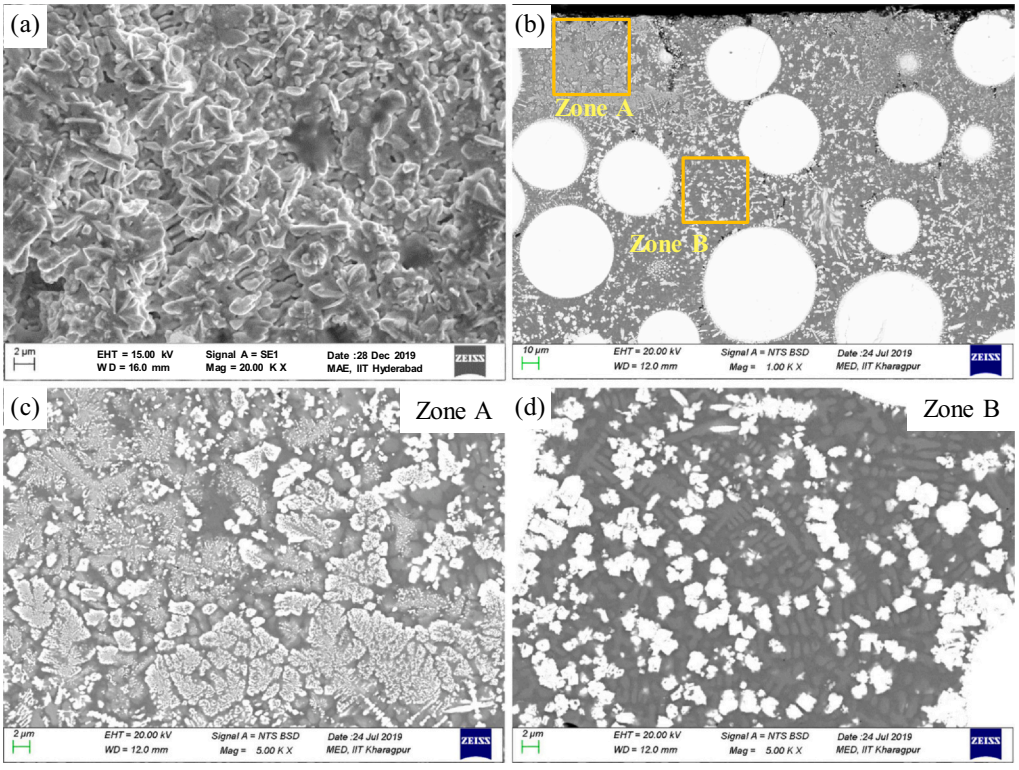

Fig. 16. Microstructure of laser polished sample (a) on surface, (b) cross-section near surface and magnified view in (c) polished zone and (d) as-deposited zone (600 W, 200 mm/min).

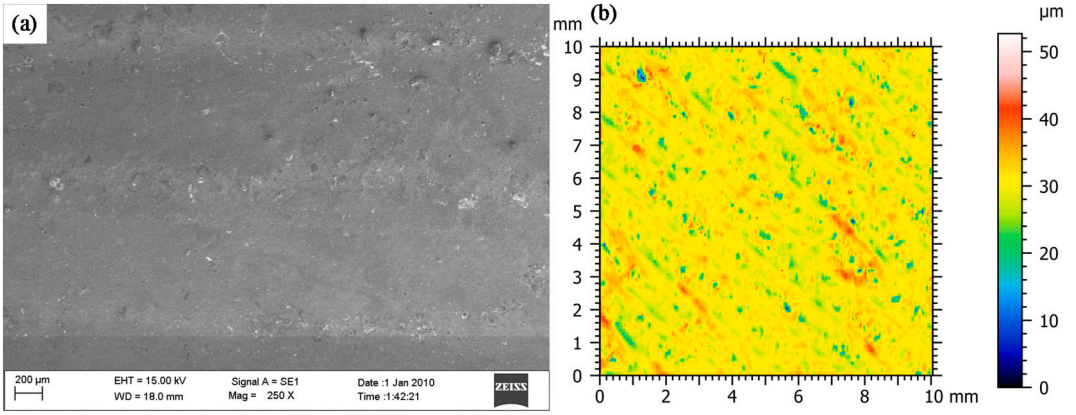

Fig. 17. Crack free surface with preheating (a) surface morphology and (b) surface topography (600 W, 2000 mm/min, 45° orientation, 500° pre-heating).

orientation. From Fig. 14(a) it can be observed that there is almost negligible variation in hardness along the depth with variation in process parameters (first indent was taken at around 50–60 µm from the top surface). However, as shown in Fig. 14(b), the hardness measured on the surface of the laser polished sample was found to be higher when compared to as-deposited and mechanically polished sample. This is due to dissociation of WC particles forming ceramic precipitates in the metal matrix which is evident from Figs. 8 and 10.

3.4. Surface cracks and its mitigation

Fig. 15 depicts the surface quality of the laser polished NiCrSiBC – 60WC ceramic-metal composite deposited by L-DED process. It can be observed that irrespective of the process parameters and the resulting molten pool life time and cooling rate, surface cracks are present for all the cases. Though laser surface remelting instigates localized heating with rapid cooling rates which refines microstructure, in case of ceramic-metal composites this develops high residual stresses due to large variation in the thermo-physical properties of metal matrix and ceramic material [21]. Table 6 summarizes the thermo-physical properties of the NiCrSiBC and WC. It can be observed that the thermal expansion coefficient of WC is almost half of the metal matrix (NiCrSiBC) with melting point as high as ~2.5 times. Therefore, during the solidification process the liquid NiCrSiBC shrinks and exerts tensile load on WC particles which nucleates crack [21,28]. Further, it may be observed from Fig. 16 that during the laser remelting process where the laser beam directly couples with the surface, WC particles were found to decompose near the surface forming dendritic structure. Fig. 16(a) and (b) shows the microstructure on the surface and across the cross-section, respectively, where the dendritic structure formed out of decomposition of WC is evident. Fig. 16(c) and (d) shows the magnified view of microstructure in the laser polished zone and the as deposited zone where a predominant dendritic structure in case of laser polished surface is evident. Gopinath et al. [29,30] reported that the dendritic structures formed out of decomposed ceramic particles are generally brittle in nature. Therefore, it may be assumed that a combined effect of residual stresses due to high cooling rate and large variation in thermo-physical properties along with decomposition of ceramic phase and formation of dendritic structure resulted in surface cracks. However, pre-heating of the substrate is reported to be the best option to control the residual stresses and mitigating the cracks [31–33]. In an earlier study, a pre-heating temperature of 500 °C has been found to control the crack formation for the same material [21]. Hence, laser polishing with the optimized parameters discussed above was carried out on the samples preheated to 500 °C. Fig. 17 shows the surface morphology and topography of the laser polished sample with pre-heating. It can be observed from Fig. 17(a) that the polished surface is free of cracks. The Ra value obtained for pre-heated sample was 1.91 µm ± 0.12, which is close to the optimum value obtained without pre-heating i.e. 1.75 µm ± 0.20. Therefore, it may be concluded that pre-heating of substrate during laser polishing in case of metal-matrix ceramic composite coating would mitigate the cracks. A thorough investigation on effect of laser polishing on surface properties like hardness, wear, corrosion and bulk mechanical properties is being carried out.

4. Conclusion

Laser surface polishing of NiCrSiBC – 60WC ceramic-metal matrix composite deposited by laser directed energy deposition process was carried out. The effect of process parameters on molten pool thermal history and surface roughness were investigated and correlated. Based on the observations, following conclusions are drawn:

1. For the same line energy input, i.e. varying laser power and scanning speed keeping their ratio constant, different molten pool thermal histories were obtained.
2. At higher laser power and scanning speed combination, heating rate and cooling rate were higher with lower molten pool lifetime.
3. Within the experimental domain, faster cooling rate resulting from higher heat input rate resulted in relatively poor surface finish due to inefficient spreading of molten pool which solidified quickly.
4. Too slow heat input rate resulted in loss of energy due to conduction, resulting in limited melting and poor surface finish.
5. An optimum combination of laser power and scanning speed exists where the molten pool gets enough time for redistributing material uniformly between peaks and valleys, yielding better surface finish.
6. Rapid cooling involved in laser polishing produces surface cracks in case of ceramic-metal composite coating which gets reduced with pre-heating of the substrate during laser deposition process.

CRediT authorship contribution statement

Amit Choudhary: Methodology, Conceptualization, Investigation, Writing - original draft, Data curation. **Abhijit Sadhu:** Methodology, Conceptualization, Investigation, Writing - original draft, Data curation. **Sagar Sarkar:** Methodology, Conceptualization, Investigation, Writing - original draft, Data curation. **Ashish Kumar Nath:** Methodology, Conceptualization, Supervision. **Muvvala Gopinath:** Conceptualization, Investigation, Writing - review & editing, Supervision, Funding acquisition.

Declaration of competing interest

The authors declare that they have no known competing financial interests or personal relationships that could have appeared to influence the work reported in this paper.

Acknowledgement

The corresponding author gratefully acknowledges the financial support from the Science and Engineering Research Board, under the startup research grant program (SRG/2019/000153). Authors also gratefully thank Department of Mechanical Engineering, IIT Kharagpur for extending the facilities which are financially supported by Department of Science and Technology, Government of India, under the FIST Program-2007 (SR/FIST/ETII-031/2007) and, Ministry of Human Resource Development and Department of Heavy Industries, Government of India, under the IMPRINT Program-2017 for Project-6917.

References

[1] S. Atamert, H.K.D.H. Bhadeshia, Comparison of the microstructures and abrasive wear properties of stellite hardfacing alloys deposited by arc welding and laser cladding, Metall. Trans. A. 20 (1989) 1037–1054.
[2] G. Xu, M. Kutsuna, Z. Liu, K. Yamada, Comparison between diode laser and TIG cladding of Co-based alloys on the SUS403 stainless steel, Surf. Coat. Technol. 201 (2006) 1138–1144.
[3] B.C. Oberlander, E. Lugscheider, Comparison of properties of coatings produced by laser cladding and conventional methods, Mater. Sci. Technol. 8 (1992) 657–665.
[4] D.A. Lesyk, S. Martinez, B.N. Mordyuk, V.V. Dzhemelinskyi, A. Lamikiz, G.I. Prokopenko, Post-processing of the Inconel 718 alloy parts fabricated by selective laser melting: effects of mechanical surface treatments on surface topography, porosity, hardness and residual stress, Surface & Coatings Technology 381 (2020) 125136.
[5] C.P. Maa, Y.C. Guana, W. Zhou, Laser polishing of additive manufactured Ti alloys, Opt. Lasers Eng. 93 (2017) 171–177.
[6] T. Deng, J. Li, Z. Zheng, Fundamental aspects and recent developments in metal surface polishing with energy beam irradiation, Int J Mach Tool Manu 148 (2020) 103472.
[7] C. Chen, H. Tsai, Fundamental study of the bulge structure generated in laser polishing process, Opt. Lasers Eng. 107 (2018) 54–61.
[8] W. Dai, J. Li, W. Zhang, Z. Zheng, Evaluation of fluences and surface characteristics in laser polishing SKD 11 tool steel, Journal of Materials Processing Tech 273 (2019) 116241.
[9] J.A. Ramos, D.L. Bourell, J.J. Beaman, Surface over-melt during laser polishing of indirect-SLS metal parts, Materials Research Society Symposium-Proceedings 758 (2002) 53–61.
[10] A. Temmler, D. Liu, J. Preußner, S. Oeser, J. Luo, R. Poprawe, J.H. Schleifenbaum, Influence of laser polishing on surface roughness and microstructural properties of the remelted surface boundary layer of tool steel H11, Mater. Des. 192 (2020) 108689.
[11] K.C. Yung, T.Y. Xiao, H.S. Choy, W.J. Wang, Z.X. Cai, Laser polishing of additive manufactured CoCr alloy components with complex surface geometry, Journal of Materials Processing Tech 262 (2018) 53–64.
[12] K.C. Yung, W.J. Wang, T.Y. Xiao, H.S. Choy, X.Y. Mo, S.S. Zhang, Z.X. Cai, Laser polishing of additive manufactured CoCr components for controlling their wettability characteristics, Surface & Coatings Technology 351 (2018) 89–98.
[13] W.J. Wang, K.C. Yung, H.S. Choy, T.Y. Xiao, Z.X. Cai, Effects of laser polishing on surface microstructure and corrosion resistance of additive manufactured CoCr alloys, Appl. Surf. Sci. 443 (2018) 167–175.
[14] S. Marimuthu, A. Triantaphyllou, M. Antar, D. Wimpenny, H. Morton, M. Beard, Laser polishing of selective laser melted components, Int J Mach Tool Manu 95 (2015) 97–104.
[15] Y. Tian, Wojciech S. Gora, A.P. Cabo, L.L. Parimi, D.P. Hand, S. Tammas-Williams, P.B. Prangnell, Material interactions in laser polishing powder bed additive manufactured Ti6Al4V components, Additive Manufacturing 20 (2018) 11–22.
[16] Y. Li, Z. Zhang, Y. Guan, Thermodynamics analysis and rapid solidification of laser polished Inconel 718 by selective laser melting, Appl. Surf. Sci. 511 (2020) 145423.
[17] S. Dadbakhsh, L. Hao, C.Y. Kong, Surface finish improvement of LMD samples using laser polishing, Virtual and Physical Prototyping 5 (4) (2010) 215–221.
[18] B. Rosa, P. Mognol, J. Hascoët, Laser polishing of additive laser manufacturing surfaces, Journal of Laser Applications 27 (2015) S29102.
[19] G.T. Hossein, J. Jhabvala, E. Boillat, T. Ivas, R. Drissi-Daoudi, R.E. Logé, An effective rule for translating optimal selective laser melting processingparameters from one material to another, Additive Manufacturing 36 (2020) 101496.
[20] D.B. Hann, J. Iammi, J. Folkes, A simple methodology for predicting laser-weld properties from material and laser parameters, J. Phys. D. Appl. Phys. 44 (2011) 445401.
[21] A. Sadhu, A. Choudhary, S. Sarkar, A.M. Nair, P. Nayak, S.D. Pawar, Gopinath Muvvala, S.K. Pal, A.K. Nath, A study on the influence of substrate preheating on mitigation of cracks in direct metal laser deposition of NiCrSiBC-60%WC ceramic coating on Inconel 718, Surface & Coatings Technology 389 (2020) 125646.
[22] M. Balbaa, S. Mekhiel, M. Elbestawi, J. McIsaac, On selective laser melting of Inconel 718: densification, surface roughness, and residual stresses, Mater. Des. 193 (2020) 108818.
[23] B. Richter, N. Blanke, C. Werner, N.D. Parab, T. Sun, F. Vollertsen, F.E. Pfefferkorn, High-speed X-ray investigation of melt dynamics during continuous-wave laser remelting of selective laser melted Co-Cr alloy, CIRP Ann. Manuf. Technol. 68 (2019) 229–232.
[24] L. Scime, J. Beuth, Melt pool geometry and morphology variability for the Inconel 718 alloy in a laser powder bed fusion additive manufacturing process, Additive Manufacturing 29 (2019) 100830.
[25] E. Toyserkani, A. Khajepour, S.F. Corbin, Laser Cladding, CRC press, 2004.
[26] M. Gopinath, S. Mullick, A.K. Nath, Development of process maps based on molten pool thermal history during laser cladding of Inconel 718/TiC metal matrix composite coatings, Surface & Coatings Technology 399 (2020) 126100.
[27] S. Zhou, X. Zeng, Q. Hu, Y. Huang, Analysis of crack behavior for Ni-based WC composite coatings by laser cladding and crack-free realization, Appl. Surf. Sci. 255 (2008) 1646–1653.
[28] W.D. Kingery, Factors affecting thermal stress resistance of ceramic materials, J. Am. Ceram. Soc. 38 (1955) 3–15.
[29] G. Muvvala, D. Patra Karmakar, A.K. Nath, In-process detection of microstructural changes in laser cladding of in-situ Inconel 718/TiC metal matrix composite coating, J. Alloys Compd. 740 (2018) 545–558.
[30] G. Muvvala, D. Patra Karmakar, A.K. Nath, Online assessment of TiC decomposition in laser cladding of metal matrix composite coating, Mater. Des. 121 (2017) 310–320.
[31] S. Zhou, X. Zeng, Growth characteristics and mechanism of carbides precipitated in WC–Fe composite coatings by laser induction hybrid rapid cladding, J. Alloys Compd. 505 (2010) 685–691.
[32] S. Zhou, X. Dai, Microstructure evolution of Fe-based WC composite coating prepared by laser induction hybrid rapid cladding, Appl. Surf. Sci. 256 (2010) 7395–7399.
[33] S. Zhou, X. Dai, H. Zheng, Analytical modeling and experimental investigation of laser induction hybrid rapid cladding for Ni-based WC composite coatings, Opt. Laser Technol. 43 (2011) 613–621.